

# Solution-Processable Covalent Organic Framework Electrolytes for All-Solid-State Li–Organic Batteries

Xing Li,<sup>#</sup> Qian Hou,<sup>#</sup> Wei Huang, Hai-Sen Xu, Xiaowei Wang, Wei Yu, Runlai Li, Kun Zhang, Lu Wang, Zhongxin Chen, Keyu Xie,\* and Kian Ping Loh\*



Cite This: *ACS Energy Lett.* 2020, 5, 3498–3506



Read Online

ACCESS |

Metrics & More

Article Recommendations

Supporting Information

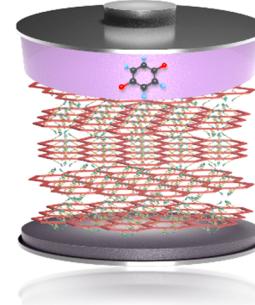
**ABSTRACT:** Solid electrolytes (SEs) are milestones in the technology roadmaps for safe and high energy density batteries. The design of organic SEs is challenged by the need to have dynamic structural fluidity for ion motion. The presence of well-ordered one-dimensional (1D) channels and stability against phase transition in covalent organic frameworks (COFs) render them potential candidates for low-temperature SEs. Herein, we demonstrate two milestones using hydrazone COF as an SE: it achieves an ion conductivity of  $10^{-5}$  S cm<sup>-1</sup> at -40 °C with a Li<sup>+</sup> transference number of 0.92 and also prevents the dissolution of small organic molecular electrode in all-solid-state batteries. Using 1,4-benzoquinone as the cathode, a lithium battery using hydrazone COF as a SE runs for 500 cycles at a steady current density of 500 mA g<sup>-1</sup> at 20 °C. Considering that hydrazone COF is readily amenable to large-scale production and facile post-synthetic modification, its use in an all-solid-state battery is highly promising.

## COF-electrolyte-based all-solid-state Li organic battery

Low-temperature  
Li<sup>+</sup> conductivity  
Up to  $10^{-5}$  S cm<sup>-1</sup> at -40 °C

Single ion conduction  
Li<sup>+</sup> transference number  
Up to 0.92

Preventing dissolution  
of organic cathode,  
1,4-benzoquinone



Covalent organic frameworks (COFs) are molecular construction kits that allow precise assembly of small organic molecules into covalent solids with built-in functionalities.<sup>1–15</sup> Their rigid structures and 1D periodic channels make them attractive as ion conductors.<sup>16–31</sup> The permanent porosity, wide structural tunability, and stability of COFs are advantageous when used as solid electrolyte (SE) compared to inorganic ion conductors such as metal oxides/sulfides; the latter are chemically difficult to modify, unstable in air, and brittle against bending.<sup>32–37</sup> However, the ion conductivities of dry organic materials are typically lower than inorganic materials. To improve conductivity, researchers have infiltrated polymers or COFs with Li salts to boost ion conductivity, giving rise to binary-ion conductors.<sup>20,22,27–29,38</sup> Single-ion conductors based on immobilizing anions on polymers or COFs were also proposed.<sup>33,39,40</sup> In spite of having ionic conductivities lower than those of binary ones, research has shown that single-ion conductors can effectively improve battery performance.<sup>41–44</sup> This is because single-ion conduction affords a Li<sup>+</sup> transference number close to unity and inhibits salt concentration gradients across the electrolyte that ultimately jeopardize battery stability. To promote the dissociation of Li salts, polymers such as polyethylene glycol (PEO) were often utilized to solvate Li ions in organic SEs,

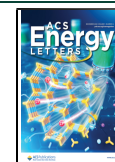
resulting in an ion conductivity that is highly dependent on the amorphicity degree and the lowest possible glass transition/melting temperature ( $T_g/T_m$ ).<sup>27,36</sup>

Because of the rigid framework structures, the  $T_g/T_m$  of COFs should surpass their decomposition temperature. Fundamentally, COF electrolytes possess a different mechanism of ion diffusion compared to linear polymer electrolytes. The enhanced ion diffusion in polymer electrolytes has been attributed to the free volume created by frustrated packing of linear polymers.<sup>45</sup> In contrast, the permanent porosity of COFs can provide abundant free volume over a wide range of temperature, thereby creating the possibility for solid-state ion conduction at a much lower temperature than the polymer. Furthermore, the pores of COFs can be functionalized with acidic groups that can coordinate and dissociate with Li ion quickly, which may allow single-Li-ion conduction at solvent-

Received: September 2, 2020

Accepted: October 12, 2020

Published: October 21, 2020



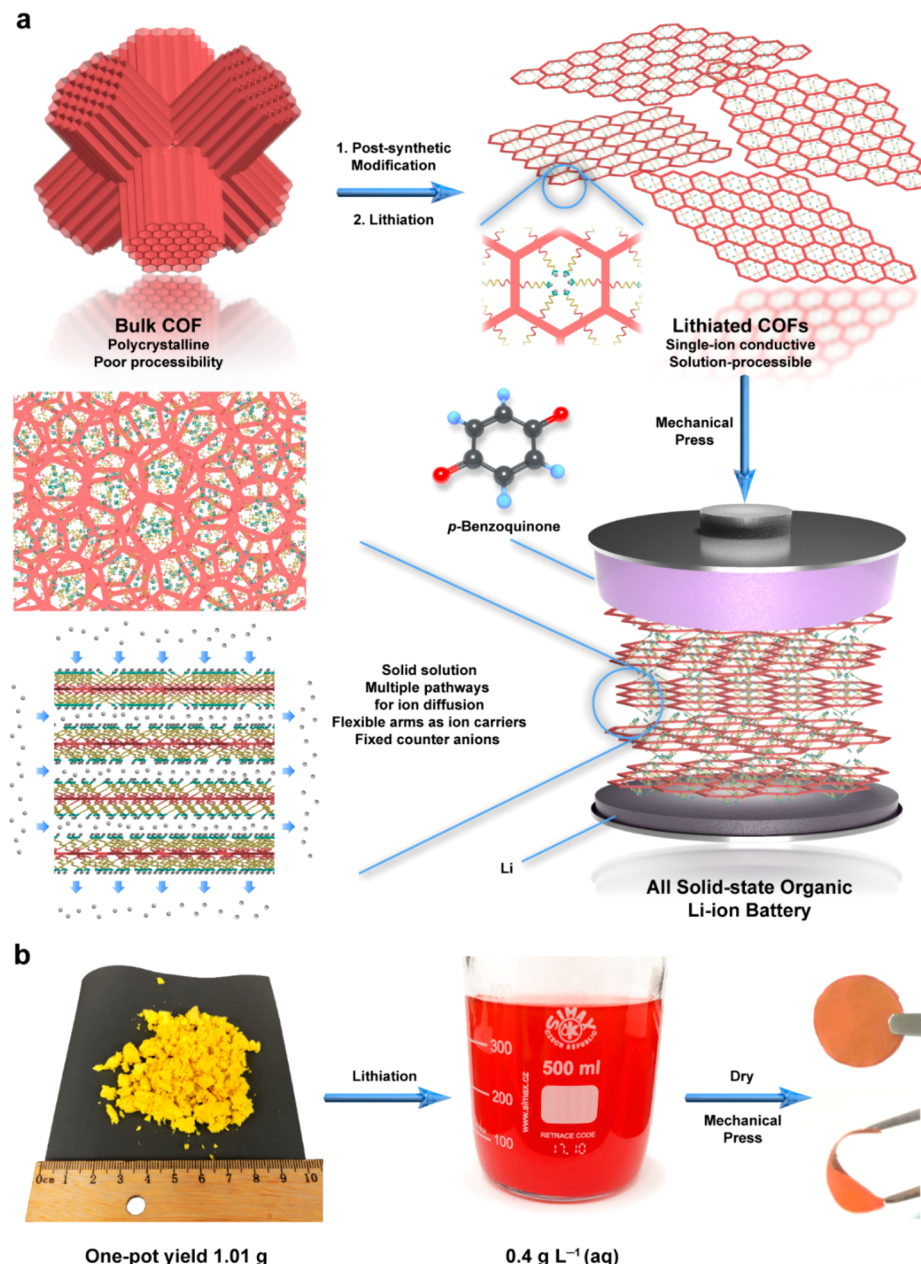


**Figure 1.** COF SE for solid-state Li ion battery. (a) Schematic illustration describing the fabrication of all-solid-state organic Li-ion battery using lithiated COF nanosheets. (b) Gram-scale preparation of COF for solid-state battery. The bulk COF powder can be processed in water and mechanically pressed into a battery separator after drying.

free conditions.<sup>26</sup> Besides, studies have shown the ion conduction can be improved when bulk 2D COFs are exfoliated into nanosheets.<sup>21,46</sup> The porous nanosheet structure enhances ion conductivity by providing enriched ion diffusion pathways (Figure 1a).

Going beyond inorganic-based battery electrodes, organic electrodes based on molecular solids with redox properties have attracted tremendous research attention because of their high specific capacity, environmental friendliness, and high safety value.<sup>47–50</sup> However, a serious drawback is the dissolution problem of the organic redox species in liquid electrolyte, which leads to fast decay of battery capacity and short cycle life. For example, the severe dissolution problem of 1,4-benzoquinone, despite its high specific capacity, is well-known.<sup>51</sup> The use of SE can potentially address the dissolution

problem provided a stable and intimate interface can be established with the organic cathode. Herein, we report a scalable and solution-processable COF platform that has the following benefits: first, it allows solvent-free ion conduction at  $-40^{\circ}\text{C}$  with a single-ion conductivity of  $10^{-5} \text{ S cm}^{-1}$ , which is unprecedented in organic-type SEs; second, it can be used as SEs and battery separators; third, it interfaces well with organic cathode made of 1,4-benzoquinone molecular solid and prevents the problem of dissolution. Considering this, we achieved an all-solid-state Li organic battery that can run for 500 cycles at a current density of  $500 \text{ mA g}^{-1}$  at  $20^{\circ}\text{C}$ .

To use COF as SE, it must be cost-efficient to synthesize.<sup>52</sup> It must also be thermally and electrochemically stable and easy to chemically modify and process. In line with these requirements, we have designed and synthesized a hydra-

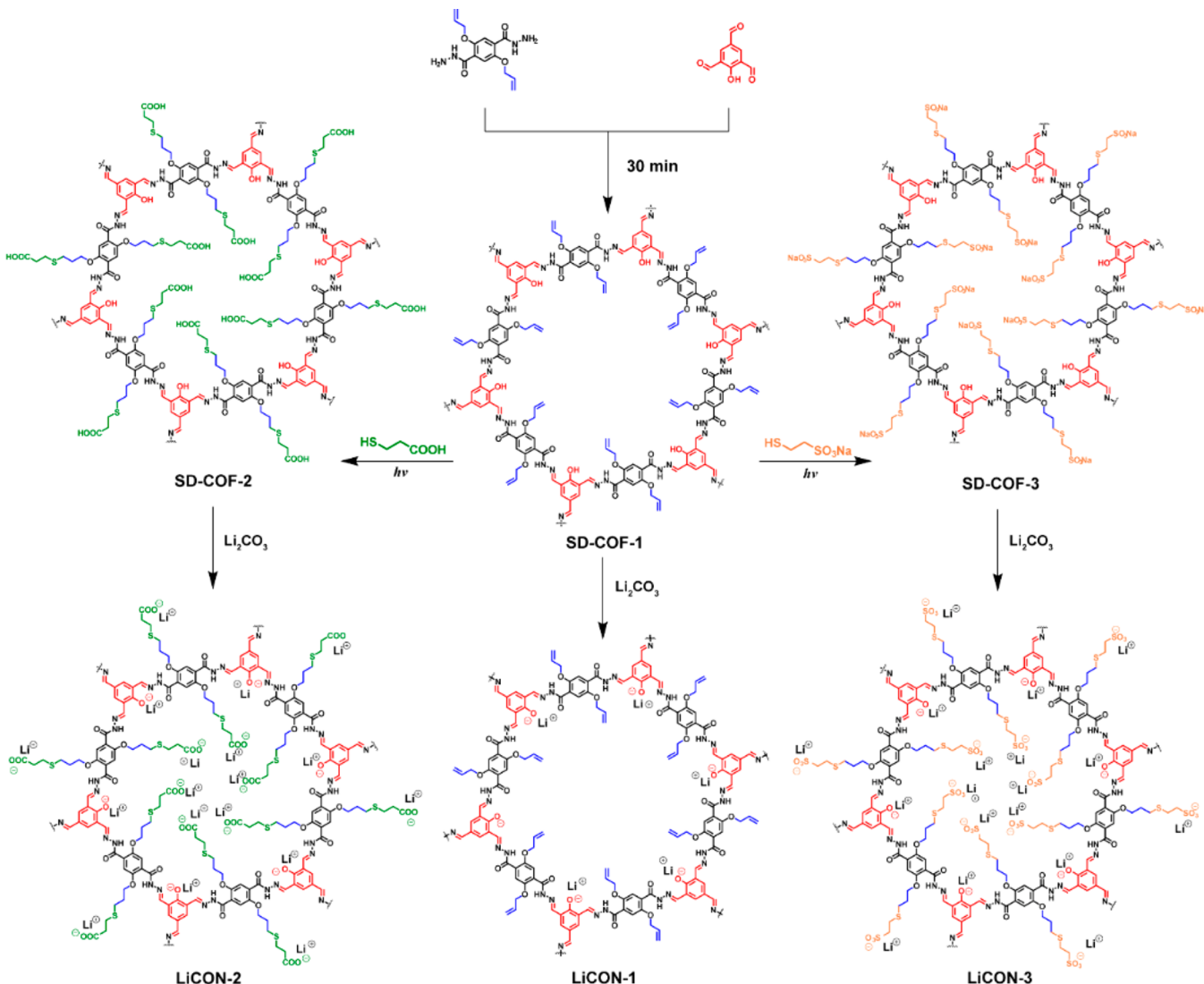


**Figure 2.** Synthesis of lithiated CONs.

zone-based COF with phenol group in the backbone functionality, and allyl group as the side chain at the channel wall. The allyl group allows post-synthetic modification with acids or salts via thiol–ene click chemistry. The thioether side chain serves to immobilize anions for single-Li-ion conduction and facilitates the dissociation of Li salts. The phenol group can be converted to a phenolic salt with lithiation; this has the effect of improving the solvation of the COFs. The charge build-up due to lithiation induces ionic repulsion between COF layers and allows them to be exfoliated readily into covalent organic nanosheets (CONs). As shown in Figures 1b and 2, SD-COF-1 was prepared in an open stirring condition by heating 2,4,6-triformylphenol and 2,5-bis(allyloxy)-terephthalohydrazide for 30 min, affording a one-pot yield of 1.01 g. SD-COF-2 and SD-COF-3 were synthesized from SD-COF-1 through photochemical thiol–ene click reaction with commercially available 3-mercaptopropanoic acid and sodium 2-mercaptopethanesulfonate, respectively. Upon treating these COFs with aqueous lithium carbonate, lithiated CONs were obtained after washing and drying. We named these lithiated CONs as LiCON-1, LiCON-2, and LiCON-3 depending on the type of side chains, as shown in Figure 2.

SD-COF-1 was produced in gram scale, and powder X-ray diffraction (PXRD) confirmed that it shows good crystallinity (Figure 3a). More details on the structure confirmation are shown in the Supporting Information (Figure S1 and discussion).

To ensure the successful connection of thiol species onto SD-COF-1, the post-synthetically modified SD-COF-2 and SD-COF-3 were characterized by solid-state CP/MAS  $^{13}\text{C}$  NMR (Figure 3d). The peak at 131.25 ppm is assigned to the secondary carbon (a) of the allyloxy side chain in SD-COF-1. After thiol–ene click reaction, the peak at 131.25 ppm decreases dramatically in SD-COF-2 and SD-COF-3, suggesting the conversion of C=C bond. Besides, a new peak at 173.51 ppm appears in COF-2, which is assigned to the carbon (b) in carboxyl group, indicating that carboxyl acid was successfully anchored in SD-COF-2. A distinct peak at 51.83 ppm observed for SD-COF-3 is assigned to the  $\alpha$ -carbon (c) of the sulfonate group, indicating the successful installation of sulfonate salt in SD-COF-3. A detailed NMR assignment is shown in Figure S3. Fourier transform infrared (FT-IR) spectra of the COFs also evidenced the successful postsynthetic modification by the appearance of C=O stretching band at 1724  $\text{cm}^{-1}$  (carboxylic

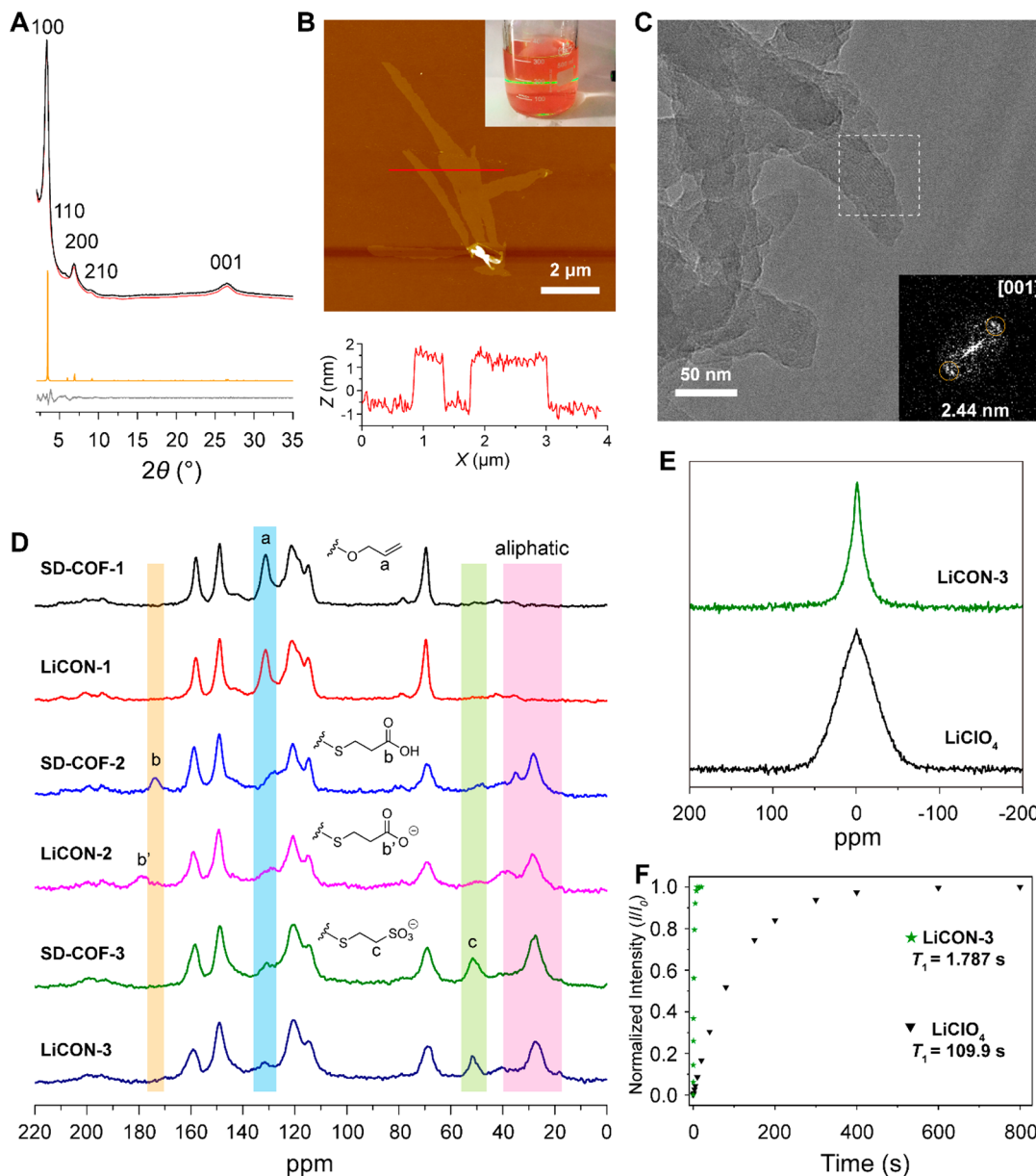


**Figure 3.** Characterization of as-prepared materials. (a) PXRD patterns of SD-COF-1 (black, experimental; red, Pawley refined; orange, simulated antiparallel stacking; gray, difference between experimental and Pawley refined PXRD). (b) AFM image of LiCON-3 (inset: LiCON-3 water dispersion shows conspicuous Tyndall effect). (c) TEM of the LiCON-3 (inset: FFT of the fringes in the selected area with  $d$ -spacing of 2.44 nm). (d) Solid-state CP/MAS  $^{13}\text{C}$  NMR characterization of as-prepared COFs and CONs. (e) Static solid-state  $^7\text{Li}$  NMR of LiCON-3 and solid LiClO<sub>4</sub> salt. (f) Saturation recovery plot of solid-state  $^7\text{Li}$  NMR spectra (green, LiCON-3; black, LiClO<sub>4</sub>).

acid) in SD-COF-2 and the S=O stretching band at  $1047\text{ cm}^{-1}$  in SD-COF-3 (Figure S4).

Upon lithiation of the phenol groups, the solution dispersibility of COFs was vastly improved. The ionic repulsion induced by lithium ions between the COF layers offsets the van der Waals interactions, allowing the COFs to be exfoliated into ultrathin organic sheets called LiCONs, which can be readily solvated because of their ionic charges (Figures 3b (inset) and S7). The thickness of LiCONs was characterized using atomic force microscope (AFM) (Figures 3b and S11). By drop casting the LiCONs dispersion in ethanol onto silica substrate, ultrathin organic nanosheets can be obtained. LiCON-1, LiCON-2, and LiCON-3 are the derivatives of the parent compound SD-COF-1, SD-COF-2, and SD-COF-3, respectively. Because of the ultrathin nature of

the exfoliated LiCONs, their crystallinity could not be observed by conventional PXRD, which agrees with previous findings of not detecting PXRD peaks on exfoliated COFs.<sup>53,54</sup> Therefore, we performed a transmission electron microscopy (TEM) study to confirm the crystallinity of LiCONs (Figures 3c and S12). The fast Fourier transform (FFT) of the TEM fringes reveals a  $d$ -spacing of 2.44 nm, which is consistent with the  $d$ -spacing of (100) planes of the COFs. Solid-state  $^{13}\text{C}$  NMR of the lithiated CONs (LiCONs) were also recorded. The spectra of LiCONs are similar to their parent COFs, suggesting the LiCONs maintain their chemical integrity. A small downfield shift is observed for the carboxylic carbon (b to b'), which is consistent with the fact that carboxylic acid is converted to Li salt upon lithiation.

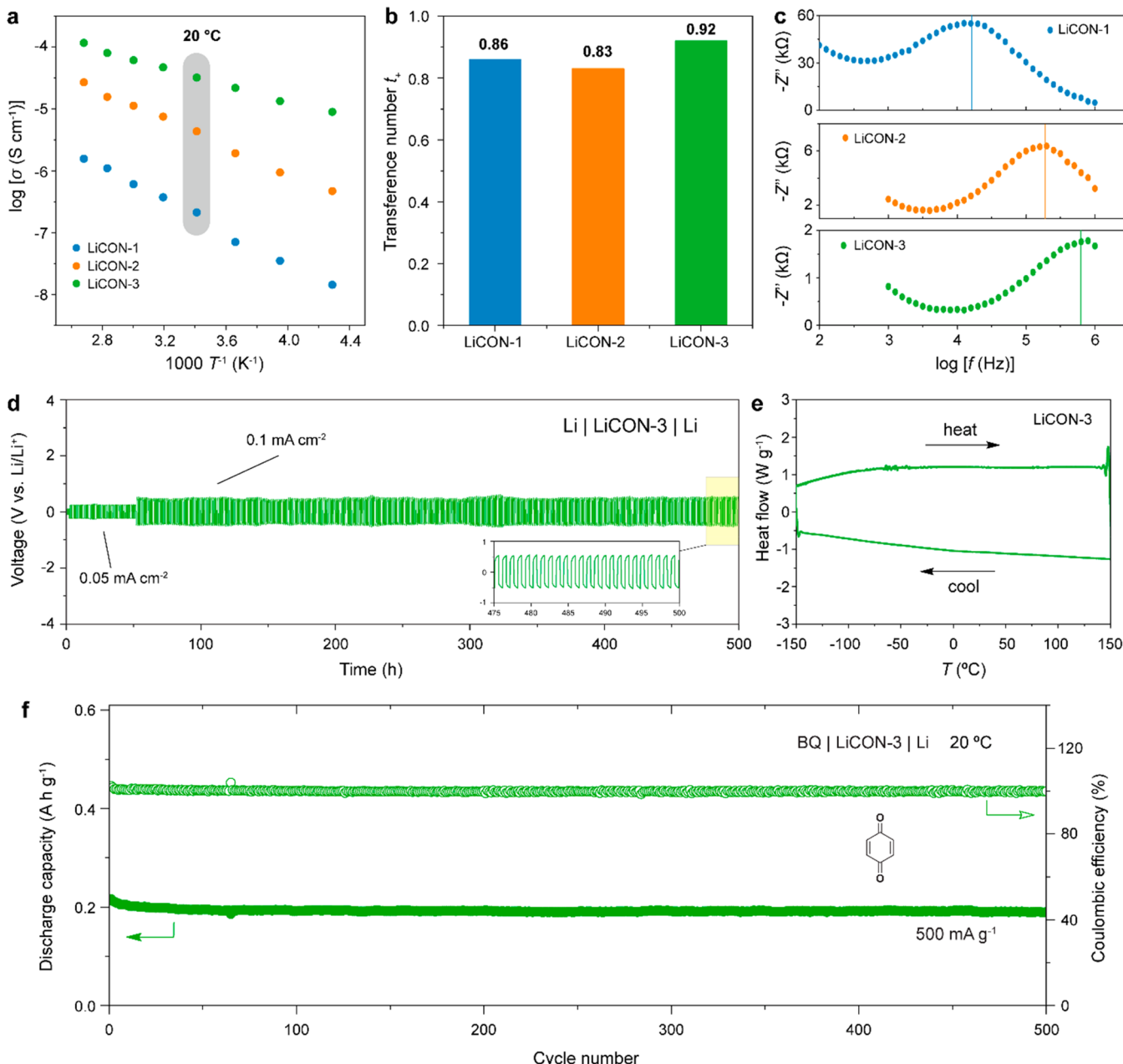


**Figure 4.** Performance of the CON SEs. (a) Arrhenius plots of the three as-prepared materials: LiCON-1, LiCON-2, and LiCON-3. (b) Li ion transference number of LiCONs. (c) Representative Debye plots of imaginary impedance as a function of  $\log f$ . (d) Li stripping–plating test of  $\text{Li} \mid \text{LiCON-3} \mid \text{Li}$  at a current density of  $0.05$  and  $0.1 \text{ mA cm}^{-2}$  for  $500$  and  $1 \text{ h}$  per cycle. (e) DSC curve of LiCON-3 from  $-150$  to  $150$   $^\circ\text{C}$ . (f) Cycling performance of all solid-state organic Li ion battery with a configuration of BQ | LiCON-3 | Li.

Using solid-state NMR, we also examined the effect of thioether side chain in facilitating Li ion dissociation. The dynamic behavior of Li ion in LiCON-3 was studied using solid-state  $^{7}\text{Li}$  NMR at  $296$  K. The static  $^{7}\text{Li}$  NMR spectrum (Figure 3e) of solid  $\text{LiClO}_4$  salt exhibits a broad peak due to the solid-state dipole–dipole and quadrupolar coupling between lithium sites, suggesting the low mobility of Li ions in  $\text{LiClO}_4$ . On the other hand, the thioether sulfur atom on the flexible side chain can help dissociate the Li salt, giving rise to a much narrower peak in the static  $^{7}\text{Li}$  NMR spectrum for LiCON-3, a signature of the highly mobile lithium ion in LiCON-3 which weakens the effect of solid-state coupling. Moreover, saturation recovery study reveals a much faster Li ion dynamics in LiCON-3, with  $T_1$  relaxation times of  $1.787$  s

for LiCON-3 and  $109.9$  s for  $\text{LiClO}_4$ , respectively (Figure 3f). These results indicate that the fast dynamics of  $\text{Li}^+$  is related to the porosity and functionalities of LiCON-3.

To test ion-conducting properties when used as true solid-state batteries, LiCONs were pressed into  $\sim 200 \mu\text{m}$  thick films without adding any Li salts or solvents (Figure 1b). The  $\text{Li}^+$  loading values in LiCON-1, LiCON-2, and LiCON-3 were assayed by inductively coupled plasma optical emission spectroscopy (ICP-OES), and are  $0.27$ ,  $2.05$ , and  $1.41$  wt % for LiCON-1, 2, and 3, respectively.

Differential scanning calorimetry (DSC) shows that CONs show no phase transition between  $-150$  and  $150$   $^\circ\text{C}$ , as confirmed by Figures 4e and S13. This ensures that COF SEs can work over a wide temperature range with no abrupt decay

of ion conductivity. The ion conductivities of LiCONs at various temperatures are shown in the Arrhenius plot from  $-40$  to  $100\text{ }^{\circ}\text{C}$  (Figure 4a). At  $20\text{ }^{\circ}\text{C}$ , LiCON-1 exhibits a low ion conductivity of  $2.13 \times 10^{-7}\text{ S cm}^{-1}$ , indicating that the strong binding with Li ions in lithium phenolate precludes fast ion conduction. To improve  $\text{Li}^{+}$  transport, we convert the framework into a cation exchange resin by incorporating anions such as carboxylate and sulfonate group with higher  $\text{Li}^{+}$  dissociation constants at the end of the flexible organic chains. Accordingly, the ionic conductivities of LiCON-2 and LiCON-3 at  $20\text{ }^{\circ}\text{C}$  increase to  $4.36 \times 10^{-6}$  and  $3.21 \times 10^{-5}\text{ S cm}^{-1}$ , respectively. In fact, even at a low lithium loading content of 1.41 wt %, LiCON-3 displays the highest ion conductivities among all reported solvent-free, organic-based single-ion conductors to date (including polymers and COFs, see Tables S1 and S2). Most impressively, LiCON-3 maintains an ion conductivity of  $0.90 \times 10^{-5}\text{ S cm}^{-1}$  at  $-40\text{ }^{\circ}\text{C}$ , a temperature regime where most organic SEs do not show any ion conductivity. This is attributed to the phase stability and flexible anion side chains for  $\text{Li}^{+}$  transport in LiCON-3. At  $100\text{ }^{\circ}\text{C}$ , LiCON-3 displays an ion conductivity of  $1.17 \times 10^{-4}\text{ S cm}^{-1}$ , suggesting that it can be used in a wide range of working temperatures. The absence of phase transition in LiCONs suggests they are a different class of SEs compared to those solvent-incorporated ones. We tried infiltrating 20 wt % of ethylene carbonate (EC) with a melting point at  $38\text{ }^{\circ}\text{C}$  into LiCON-3. The ion conductivity increases to  $1.26 \times 10^{-4}\text{ S cm}^{-1}$  at  $60\text{ }^{\circ}\text{C}$ , which is higher than that of solvent-free LiCON-3 ( $6.11 \times 10^{-5}\text{ S cm}^{-1}$  at  $60\text{ }^{\circ}\text{C}$ ). However, the ion conductivity dramatically decreases to  $9.06 \times 10^{-6}\text{ S cm}^{-1}$  at  $20\text{ }^{\circ}\text{C}$  when the temperature drops below the melting point of EC (Figure S27).

The activation energies for ion hopping in LiCONs are derived from the Arrhenius plot in Figure 4a. The activation energies of LiCON-1, LiCON-2, and LiCON-3, are 0.25, 0.22, and 0.13 eV, respectively. These activation energies are generally lower compared to previously reported COFs (Table S1), and the origin can be traced to the ion-permeable channels in restacked 2D LiCON with its flexible anion side chains promoting ion hopping. The low activation energies of LiCONs are beneficial for ion conduction at low temperatures. As shown in the Arrhenius plot, the ion conductivity decays very slowly with falling temperature. Most importantly, CON does not show glass transition that is typical of linear polymer-based SEs; thus, it is not affected by crystallization-induced decrease in ion conductivity. The Debye plot of imaginary impedance as a function of frequency reveals the relaxation time for ion hopping (Figure 4c). The frequency of the Debye peak is characteristic of the relaxation time. As shown in Figure 4c, the Debye peak of LiCON-3 appears at the highest frequency among the three LiCONs, indicating that it has the fastest relaxation process. To evaluate the contribution of lithium ions in ion migration fraction, the single-ion conduction in LiCONs is confirmed by dc polarization and ac impedance measurements (Figure S14). The lithium transference number is determined to be 0.86, 0.83, and 0.92 for LiCON-1, LiCON-2 and LiCON-3, respectively at  $20\text{ }^{\circ}\text{C}$  (Figure 4b). The high transference number of LiCONs suggests that the materials are conductive for only cations and not anions. The stability tests of the LiCONs were also conducted, including the electrochemical stability window, performance durability, and thermogravimetric analysis

(Figures S15–S18). LiCON-3 exhibits an electrochemical window of  $1.6$ – $4.3\text{ V}$  versus  $\text{Li}/\text{Li}^{+}$ .

The similarities and differences of ion conduction behaviors in LiCONs allow us to perform structure–property correlation analysis. First, all LiCONs are single-Li-ion conductive, indicating that immobilization of anions onto the COF backbone can induce the single conduction of cations. Second, LiCON-3 exhibits the highest ion conductivity among LiCONs, followed by LiCON-2 and then LiCON-1, suggesting that ion conductivity can be enhanced by using Li salts derived from stronger acids. This is because the counteranion plays an important role in promoting Li ion dissociation. The anions are phenolate, carboxylate, and sulfonate in LiCON-1, 2, and 3, respectively, which show increasing acidity for their acidic counterpart. Therefore, LiCON-3 with sulfonate groups has the largest dissociation constant of Li ions, giving rise to the highest ion conductivity among the LiCONs. Last but not least, we also found exfoliation is beneficial for the ion conduction. The ion conductivity of unexfoliated SD-COF-3 functionalized with sulfonate salts is  $3.1 \times 10^{-6}\text{ S cm}^{-1}$  at  $20\text{ }^{\circ}\text{C}$ , which is around one tenth of that of LiCON-3 (Figure S20). It is speculated that exfoliation of COF may create more diffusion pathways for enhancing ion transport as shown in Figure 1a.

Having identified LiCON-3 as the best performer among all our COFs, we tested its stability under different conditions. In a  $\text{Li} \mid \text{Li}-\text{CON-3} \mid \text{Li}$  symmetric cell configuration, the Li stripping–plating test can be stably recycled for 500 h (1 h per cycle) at a relatively high current density of 0.05 and  $0.1\text{ mA cm}^{-2}$  (Figure 4d). The symmetric cell exhibits no obvious increase or irreversible fluctuation of overpotential.

1,4-Benzoquinone (BQ) is attractive for use as organic cathode in Li ion battery on account of its high specific energy capacity and low cost.<sup>47,51</sup> However, the dissolution of 1,4-benzoquinone is severe in liquid electrolyte, resulting in fast decay of the specific energy capacity and poor cycling performance of the battery. Solvent-free COF SEs provide a solution to this problem. As a proof-of-concept, we assembled  $\text{BQ} \mid \text{LiCON-3} \mid \text{Li}$  all-solid-state organic Li ion battery and tested its cycling performance. Solid-state batteries assembled based on LiCON-3 exhibit great stability. At  $20\text{ }^{\circ}\text{C}$ , the battery can run for 500 cycles at a current density of  $500\text{ mA g}^{-1}$  with 87.7% retention of initial capacity (Figure 4f). The batteries also show good rate performance with moderate decay of discharge capacity with increasing current density to  $1\text{ A g}^{-1}$  and negligible loss of capacity when the current density returns to  $0.25\text{ A g}^{-1}$ . In contrast, the liquid electrolyte-based BQ battery exhibited a fast decay of capacity in 10 cycles (Figure S24).

To conclude, we have designed and synthesized COFs that can be used as SEs, leading to impressive cycle stability of cathodes constructed from quinone-based organic molecules. Our COF platform features facile post-synthetic modification and can be converted into cation exchange resins via thiol–ene click chemistry, and further exfoliated into CONs by lithiation. CON SEs functionalized with sulfonate groups exhibit a high  $\text{Li}^{+}$  transference number of 0.92 at  $20\text{ }^{\circ}\text{C}$ , and a high ion conductivity that can be sustained down to low temperature ( $-40\text{ }^{\circ}\text{C}$ ). In addition, their anchored flexible anions facilitate single-ion conduction under solvent-free conditions. The wide electrochemical window, high thermal and water stability of CON SEs render them useful as SE and separators in all-solid-state Li organic batteries.

**■ ASSOCIATED CONTENT****SI Supporting Information**

The Supporting Information is available free of charge at <https://pubs.acs.org/doi/10.1021/acsenergylett.0c01889>.

General information on instruments and methods; synthesis procedures; preparation of COF SE and solid battery; characterizations including PXRD, nitrogen sorption, FTIR, solid-state  $^{13}\text{C}$  NMR, SEM, TEM, AFM, TGA, EIS, CV, and LSV; battery performance; Figures S1–S27; and Tables S1 and S2 ([PDF](#))

**■ AUTHOR INFORMATION****Corresponding Authors**

**Keyu Xie** — State Key Laboratory of Solidification Processing, Center for Nano Energy Materials, Northwestern Polytechnical University and Shaanxi Joint Laboratory of Graphene (NPU), Xi'an 710072, P.R. China; Email: [kxyie@nwpu.edu.cn](mailto:kxyie@nwpu.edu.cn)

**Kian Ping Loh** — Frontiers Science Center for Flexible Electronics (FSCFE), Northwestern Polytechnical University (NPU), Xi'an 710072, China; Department of Chemistry, National University of Singapore, Singapore 117543;  [0000-0002-1491-743X](https://orcid.org/0000-0002-1491-743X); Email: [chmlohp@nus.edu.sg](mailto:chmlohp@nus.edu.sg)

**Authors**

**Xing Li** — Department of Chemistry, National University of Singapore, Singapore 117543;  [0000-0002-5470-1043](https://orcid.org/0000-0002-5470-1043)

**Qian Hou** — State Key Laboratory of Solidification Processing, Center for Nano Energy Materials, Northwestern Polytechnical University and Shaanxi Joint Laboratory of Graphene (NPU), Xi'an 710072, P.R. China;  [0000-0002-9436-5216](https://orcid.org/0000-0002-9436-5216)

**Wei Huang** — State Key Laboratory of Solidification Processing, Center for Nano Energy Materials, Northwestern Polytechnical University and Shaanxi Joint Laboratory of Graphene (NPU), Xi'an 710072, P.R. China; Frontiers Science Center for Flexible Electronics (FSCFE), Northwestern Polytechnical University (NPU), Xi'an 710072, China

**Hai-Sen Xu** — Department of Chemistry, National University of Singapore, Singapore 117543;  [0000-0003-4137-9005](https://orcid.org/0000-0003-4137-9005)

**Xiaowei Wang** — Department of Chemistry, National University of Singapore, Singapore 117543;  [0000-0002-7542-6108](https://orcid.org/0000-0002-7542-6108)

**Wei Yu** — Department of Chemistry, National University of Singapore, Singapore 117543;  [0000-0003-3468-3439](https://orcid.org/0000-0003-3468-3439)

**Runlai Li** — Department of Chemistry, National University of Singapore, Singapore 117543;  [0000-0002-1857-2037](https://orcid.org/0000-0002-1857-2037)

**Kun Zhang** — State Key Laboratory of Solidification Processing, Center for Nano Energy Materials, Northwestern Polytechnical University and Shaanxi Joint Laboratory of Graphene (NPU), Xi'an 710072, P.R. China; Department of Chemistry, National University of Singapore, Singapore 117543;  [0000-0002-6877-8068](https://orcid.org/0000-0002-6877-8068)

**Lu Wang** — Department of Chemistry, National University of Singapore, Singapore 117543

**Zhongxin Chen** — Department of Chemistry, National University of Singapore, Singapore 117543;  [0000-0001-6153-5381](https://orcid.org/0000-0001-6153-5381)

Complete contact information is available at:

<https://pubs.acs.org/10.1021/acsenergylett.0c01889>

**Author Contributions**

#X.L. and Q.H. contributed equally.

**Notes**

The authors declare no competing financial interest.

**■ ACKNOWLEDGMENTS**

The authors acknowledge the financial support provided by the 381 National Natural Science Foundation of China (51974256 and 52034011), the Outstanding Young Scholars of Shaanxi (2019JC-12), and the Fundamental Research Funds for the Central Universities (20GH020137 and 3102019JC005). K.P.L. acknowledges NRF-CRP grant “Two-Dimensional Covalent Organic Framework: Synthesis and Applications,” Grant Number NRF-CRP16-2015-02, funded by National Research Foundation, Prime Minister’s Office, Singapore.

**■ REFERENCES**

- (1) Diercks, C. S.; Yaghi, O. M. The atom, the molecule, and the covalent organic framework. *Science* **2017**, *355*, No. eaal1585.
- (2) Kandambeth, S.; Dey, K.; Banerjee, R. Covalent Organic Frameworks: Chemistry beyond the Structure. *J. Am. Chem. Soc.* **2019**, *141*, 1807–1822.
- (3) Chen, X.; Geng, K.; Liu, R.; Tan, K. T.; Gong, Y.; Li, Z.; Tao, S.; Jiang, Q.; Jiang, D. Covalent Organic Frameworks: Chemical Approaches to Designer Structures and Built-In Functions. *Angew. Chem., Int. Ed.* **2020**, *59*, 5050.
- (4) Segura, J. L.; Mancheno, M. J.; Zamora, F. Covalent organic frameworks based on Schiff-base chemistry: synthesis, properties and potential applications. *Chem. Soc. Rev.* **2016**, *45*, 5635–5671.
- (5) Segura, J. L.; Royuela, S.; Mar Ramos, M. Post-synthetic modification of covalent organic frameworks. *Chem. Soc. Rev.* **2019**, *48*, 3903–3945.
- (6) Mandal, A. K.; Mahmood, J.; Baek, J.-B. Two-Dimensional Covalent Organic Frameworks for Optoelectronics and Energy Storage. *ChemNanoMat* **2017**, *3*, 373–391.
- (7) DeBlase, C. R.; Silberstein, K. E.; Truong, T.-T.; Abruna, H. D.; Dichtel, W. R.  $\beta$ -Ketoenamine-Linked Covalent Organic Frameworks Capable of Pseudocapacitive Energy Storage. *J. Am. Chem. Soc.* **2013**, *135*, 16821–16824.
- (8) Montoro, C.; Rodríguez-San-Miguel, D.; Polo, E.; Escudero-Cid, R.; Ruiz-González, M. L.; Navarro, J. A. R.; Ocón, P.; Zamora, F. Ionic Conductivity and Potential Application for Fuel Cell of a Modified Imine-Based Covalent Organic Framework. *J. Am. Chem. Soc.* **2017**, *139*, 10079–10086.
- (9) Mulzer, C. R.; Shen, L.; Bisbey, R. P.; McKone, J. R.; Zhang, N.; Abruna, H. D.; Dichtel, W. R. Superior Charge Storage and Power Density of a Conducting Polymer-Modified Covalent Organic Framework. *ACS Cent. Sci.* **2016**, *2*, 667–673.
- (10) Liu, H.; Chu, J.; Yin, Z.; Cai, X.; Zhuang, L.; Deng, H. Covalent Organic Frameworks Linked by Amine Bonding for Concerted Electrochemical Reduction of CO<sub>2</sub>. *Chem.* **2018**, *4*, 1696–1709.
- (11) Zhang, L.; Wang, S.; Zhou, Y.; Wang, C.; Zhang, X.-Z.; Deng, H. Covalent Organic Frameworks as Favorable Constructs for Photodynamic Therapy. *Angew. Chem.* **2019**, *131*, 14351–14356.
- (12) Li, X.; Yadav, P.; Loh, K. P. Function-oriented synthesis of two-dimensional (2D) covalent organic frameworks – from 3D solids to 2D sheets. *Chem. Soc. Rev.* **2020**, *49*, 4835–4866.
- (13) Vitaku, E.; Gannett, C. N.; Carpenter, K. L.; Shen, L.; Abruna, H. D.; Dichtel, W. R. Phenazine-Based Covalent Organic Framework Cathode Materials with High Energy and Power Densities. *J. Am. Chem. Soc.* **2020**, *142*, 16–20.
- (14) Mahmood, J.; Ahmad, I.; Jung, M.; Seo, J.-M.; Yu, S.-Y.; Noh, H.-J.; Kim, Y. H.; Shin, H.-J.; Baek, J.-B. Two-dimensional amine and hydroxy functionalized fused aromatic covalent organic framework. *Communications Chemistry* **2020**, *3*, 31.

- (15) Li, X.; Wang, H.; Chen, Z.; Xu, H.-S.; Yu, W.; Liu, C.; Wang, X.; Zhang, K.; Xie, K.; Loh, K. P. Covalent-Organic-Framework-Based Li-CO<sub>2</sub> Batteries. *Adv. Mater.* **2019**, *31*, 1905879.
- (16) Li, X.; Loh, K. P. Recent Progress in Covalent Organic Frameworks as Solid-State Ion Conductors. *ACS Materials Letters* **2019**, *1*, 327–335.
- (17) Miner, E. M.; Dinca, M. Metal- and covalent-organic frameworks as solid-state electrolytes for metal-ion batteries. *Philos. Trans. R. Soc., A* **2019**, *377*, 20180225.
- (18) Du, Y.; Yang, H.; Whiteley, J. M.; Wan, S.; Jin, Y.; Lee, S.-H.; Zhang, W. Ionic Covalent Organic Frameworks with Spiroborate Linkage. *Angew. Chem., Int. Ed.* **2016**, *55*, 1737–1741.
- (19) Vazquez-Molina, D. A.; Mohammad-Pour, G. S.; Lee, C.; Logan, M. W.; Duan, X.; Harper, J. K.; Uribe-Romo, F. J. Mechanically Shaped Two-Dimensional Covalent Organic Frameworks Reveal Crystallographic Alignment and Fast Li-Ion Conductivity. *J. Am. Chem. Soc.* **2016**, *138*, 9767–9770.
- (20) Zhang, Y.; Duan, J.; Ma, D.; Li, P.; Li, S.; Li, H.; Zhou, J.; Ma, X.; Feng, X.; Wang, B. Three-Dimensional Anionic Cyclodextrin-Based Covalent Organic Frameworks. *Angew. Chem., Int. Ed.* **2017**, *56*, 16313–16317.
- (21) Chen, H.; Tu, H.; Hu, C.; Liu, Y.; Dong, D.; Sun, Y.; Dai, Y.; Wang, S.; Qian, H.; Lin, Z.; Chen, L. Cationic Covalent Organic Framework Nanosheets for Fast Li-Ion Conduction. *J. Am. Chem. Soc.* **2018**, *140*, 896–899.
- (22) Xu, Q.; Tao, S.; Jiang, Q.; Jiang, D. Ion Conduction in Polyelectrolyte Covalent Organic Frameworks. *J. Am. Chem. Soc.* **2018**, *140*, 7429–7432.
- (23) Dong, D.; Zhang, H.; Zhou, B.; Sun, Y.; Zhang, H.; Cao, M.; Li, J.; Zhou, H.; Qian, H.; Lin, Z.; Chen, H. Porous covalent organic frameworks for high transference number polymer-based electrolytes. *Chem. Commun.* **2019**, *55*, 1458–1461.
- (24) Guo, Z.; Zhang, Y.; Dong, Y.; Li, J.; Li, S.; Shao, P.; Feng, X.; Wang, B. Fast Ion Transport Pathway Provided by Polyethylene Glycol Confined in Covalent Organic Frameworks. *J. Am. Chem. Soc.* **2019**, *141*, 1923–1927.
- (25) Hu, Y.; Dunlap, N.; Wan, S.; Lu, S.; Huang, S.; Sellinger, I.; Ortiz, M.; Jin, Y.; Lee, S.-h.; Zhang, W. Crystalline Lithium Imidazolate Covalent Organic Frameworks with High Li-Ion Conductivity. *J. Am. Chem. Soc.* **2019**, *141*, 7518–7525.
- (26) Jeong, K.; Park, S.; Jung, G. Y.; Kim, S. H.; Lee, Y.-H.; Kwak, S. K.; Lee, S.-Y. Solvent-Free, Single Lithium-Ion Conducting Covalent Organic Frameworks. *J. Am. Chem. Soc.* **2019**, *141*, 5880–5885.
- (27) Zhang, G.; Hong, Y.-I.; Nishiyama, Y.; Bai, S.; Kitagawa, S.; Horike, S. Accumulation of Glassy Poly(ethylene oxide) Anchored in a Covalent Organic Framework as a Solid-State Li<sup>+</sup> Electrolyte. *J. Am. Chem. Soc.* **2019**, *141*, 1227–1234.
- (28) Li, Z.; Liu, Z.-W.; Li, Z.; Wang, T.-X.; Zhao, F.; Ding, X.; Feng, W.; Han, B.-H. Defective 2D Covalent Organic Frameworks for Postfunctionalization. *Adv. Funct. Mater.* **2020**, *30*, 1909267.
- (29) Zhai, L.; Tong, B.; Chen, W.; Wu, Z.; Soutis, C.; Zhu, G.; Jiang, D.; Cui, S.; Mi, L. Bromine Functionalized Covalent Organic Frameworks for Efficient Triboelectric Nanogenerator. *Chem. - Eur. J.* **2020**, *26*, 5784.
- (30) Xu, Q.; Tao, S.; Jiang, Q.; Jiang, D. Designing Covalent Organic Frameworks with a Tailored Ionic Interface for Ion Transport across One-Dimensional Channels. *Angew. Chem., Int. Ed.* **2020**, *59*, 4557–4563.
- (31) Zhang, K.; Zhang, B.; Weng, M.; Zheng, J.; Li, S.; Pan, F. Lithium ion diffusion mechanism in covalent organic framework based solid state electrolyte. *Phys. Chem. Chem. Phys.* **2019**, *21*, 9883–9888.
- (32) Manthiram, A.; Yu, X.; Wang, S. Lithium battery chemistries enabled by solid-state electrolytes. *Nat. Rev. Mater.* **2017**, *2*, 16103.
- (33) Zhang, H.; Li, C.; Piszzc, M.; Coya, E.; Rojo, T.; Rodriguez-Martinez, L. M.; Armand, M.; Zhou, Z. Single lithium-ion conducting solid polymer electrolytes: advances and perspectives. *Chem. Soc. Rev.* **2017**, *46*, 797–815.
- (34) Long, L.; Wang, S.; Xiao, M.; Meng, Y. Polymer electrolytes for lithium polymer batteries. *J. Mater. Chem. A* **2016**, *4*, 10038–10069.
- (35) Kato, Y.; Hori, S.; Saito, T.; Suzuki, K.; Hirayama, M.; Mitsui, A.; Yonemura, M.; Iba, H.; Kanno, R. High-power all-solid-state batteries using sulfide superionic conductors. *Nat. Energy* **2016**, *1*, 16030.
- (36) Bouchet, R.; Maria, S.; Meziane, R.; Aboulaich, A.; Lienafa, L.; Bonnet, J.-P.; Phan, T. N. T.; Bertin, D.; Gigmes, D.; Devaux, D.; Denoyel, R.; Armand, M. Single-ion BAB triblock copolymers as highly efficient electrolytes for lithium-metal batteries. *Nat. Mater.* **2013**, *12*, 452.
- (37) Lopez, J.; Mackanic, D. G.; Cui, Y.; Bao, Z. Designing polymers for advanced battery chemistries. *Nat. Rev. Mater.* **2019**, *4*, 312–330.
- (38) Berthier, C.; Gorecki, W.; Minier, M.; Armand, M. B.; Chabagno, J. M.; Rigaud, P. Microscopic investigation of ionic conductivity in alkali metal salts-poly(ethylene oxide) adducts. *Solid State Ionics* **1983**, *11*, 91–95.
- (39) Cheng, X.; Pan, J.; Zhao, Y.; Liao, M.; Peng, H. Gel Polymer Electrolytes for Electrochemical Energy Storage. *Adv. Energy Mater.* **2018**, *8*, 1702184.
- (40) Shin, D.-M.; Bachman, J. E.; Taylor, M. K.; Kamcev, J.; Park, J. G.; Ziebel, M. E.; Velasquez, E.; Jarenwattananon, N. N.; Sethi, G. K.; Cui, Y.; Long, J. R. A Single-Ion Conducting Borate Network Polymer as a Viable Quasi-Solid Electrolyte for Lithium Metal Batteries. *Adv. Mater.* **2020**, *32*, 1905771.
- (41) Kobayashi, N.; Uchiyama, M.; Tsuchida, E. Poly[lithium methacrylate-co-oligo(oxyethylene)methacrylate] as a solid electrolyte with high ionic conductivity. *Solid State Ionics* **1985**, *17*, 307–311.
- (42) Doyle, M.; Fuller, T. F.; Newman, J. The importance of the lithium ion transference number in lithium/polymer cells. *Electrochim. Acta* **1994**, *39*, 2073–2081.
- (43) Doyle, M.; Newman, J. The use of mathematical modeling in the design of lithium/polymer battery systems. *Electrochim. Acta* **1995**, *40*, 2191–2196.
- (44) Rosso, M.; Brissot, C.; Teyssot, A.; Dollé, M.; Sammier, L.; Tarascon, J.-M.; Bouchet, R.; Lascaud, S. Dendrite short-circuit and fuse effect on Li/polymer/Li cells. *Electrochim. Acta* **2006**, *51*, 5334–5340.
- (45) Wang, Y.; Agapov, A. L.; Fan, F.; Hong, K.; Yu, X.; Mays, J.; Sokolov, A. P. Decoupling of Ionic Transport from Segmental Relaxation in Polymer Electrolytes. *Phys. Rev. Lett.* **2012**, *108*, 088303.
- (46) Wang, S.; Wang, Q.; Shao, P.; Han, Y.; Gao, X.; Ma, L.; Yuan, S.; Ma, X.; Zhou, J.; Feng, X.; Wang, B. Exfoliation of Covalent Organic Frameworks into Few-Layer Redox-Active Nanosheets as Cathode Materials for Lithium-Ion Batteries. *J. Am. Chem. Soc.* **2017**, *139*, 4258–4261.
- (47) Häupler, B.; Wild, A.; Schubert, U. S. Carbonyls: Powerful Organic Materials for Secondary Batteries. *Adv. Energy Mater.* **2015**, *5*, 1402034.
- (48) Xie, J.; Zhang, Q. Recent progress in rechargeable lithium batteries with organic materials as promising electrodes. *J. Mater. Chem. A* **2016**, *4*, 7091–7106.
- (49) Lu, Y.; Chen, J. Prospects of organic electrode materials for practical lithium batteries. *Nat. Rev. Chem.* **2020**, *4*, 127–142.
- (50) Heiska, J.; Nisula, M.; Karppinen, M. Organic electrode materials with solid-state battery technology. *J. Mater. Chem. A* **2019**, *7*, 18735–18758.
- (51) Wu, Y.; Zeng, R.; Nan, J.; Shu, D.; Qiu, Y.; Chou, S.-L. Quinone Electrode Materials for Rechargeable Lithium/Sodium Ion Batteries. *Adv. Energy Mater.* **2017**, *7*, 1700278.
- (52) Li, X.; Qiao, J.; Chee, S. W.; Xu, H.-S.; Zhao, X.; Choi, H. S.; Yu, W.; Quek, S. Y.; Mirsaidov, U.; Loh, K. P. Rapid, Scalable Construction of Highly Crystalline Acylhydrazone Two-Dimensional Covalent Organic Frameworks via Dipole-Induced Antiparallel Stacking. *J. Am. Chem. Soc.* **2020**, *142*, 4932–4943.
- (53) Liu, W.; Li, X.; Wang, C.; Pan, H.; Liu, W.; Wang, K.; Zeng, Q.; Wang, R.; Jiang, J. A Scalable General Synthetic Approach toward Ultrathin Imine-Linked Two-Dimensional Covalent Organic Frame-

work Nanosheets for Photocatalytic CO<sub>2</sub> Reduction. *J. Am. Chem. Soc.* **2019**, *141*, 17431–17440.

(54) Yang, L.; Guo, Q.; Kang, H.; Chen, R.; Liu, Y.; Wei, D. Self-Controlled Growth of Covalent Organic Frameworks by Repolymerization. *Chem. Mater.* **2020**, *32*, 5634–5640.